



Degradation efficiency of $Mg_{65}Cu_{25-x}Ag_xY_{10}$ nanoporous dealloyed ribbons on pesticide wastewater

Qing XIA, Shi-yao HE, Wei ZHANG, Qing-chun XIANG, Ying-dong QU, Ying-lei REN, Ke-qiang QIU

School of Materials Science and Engineering, Shenyang University of Technology, Shenyang 110870, China

Received 24 April 2021; accepted 8 December 2021

Abstract: Dealloyed ribbons with a layer of networked nanoporous structure of different pore sizes were fabricated by dealloying the as-spun $Mg_{65}Cu_{25-x}Ag_xY_{10}$ ($x=0, 5, 10$, at.%) ribbons in dilute H_2SO_4 solution in order to enhance the degradation efficiency of pesticide wastewater. Compared to the as-spun ribbons, it is found that the dealloyed ribbons with the networked nanoporous structure exhibit higher degradation efficiency due to their large specific surface areas and enough active sites for the degradation process. Both the average pore sizes of the nanoporous structure and the degradation efficiency of the pesticide wastewater increase with the increase of Ag addition in the dealloyed ribbons. The maximum degradation efficiency up to 95.8% is obtained for the $Mg_{65}Cu_{15}Ag_{10}Y_{10}$ dealloyed ribbon under the optimal conditions of pH being 3, the initial cis-cypermethrin concentration being 500 mg/L, and the dosage of dealloyed ribbon being 1.33 g/L.

Key words: networked nanoporous structure; MgCu-based amorphous ribbon; dealloying; cis-cypermethrin wastewater; degradation efficiency

1 Introduction

The production and use of pesticides have caused a large amount of wastewater discharged into the environment, thus bringing about the problem of serious environmental pollution. The complex structure of pesticide is too stable to be self-degraded in the natural environment [1], which results in a long persistence of high toxicity and a serious threat to human health and animal survival. Therefore, it is urgent to degrade pesticide wastewater to avoid toxic substances accumulated in the environment. Many methods have been used to degrade different kinds of wastewater, such as flocculation [2], advanced oxidation process [3–5] and electrochemistry [6], and reduction. Among all these methods, the reduction method is a simple and environment-friendly approach to degrade

wastewater, in which zero-valent metals are often used to treat pesticide wastewater [7,8]. Because zero-valent Mg is relatively low in cost and has fast degradation rates, it is also applied to treating wastewater in the reduction method [9,10]. When Mg powder is added to a solution as the catalytic material, it is usually consumed to a large amount and will lose its catalytic capacity due to its poor corrosion resistance [11]. Solving this problem needs to search a new method to take advantage of zero-valent Mg as catalytic materials. Fortunately, Mg-based amorphous alloys are the candidates to solve this problem due to their better corrosion resistance. What's more, amorphous alloys generally have higher free energy and surface activity [12,13], suitable for being used as catalysts. Therefore, amorphous alloys show not only higher degradation efficiency but also longer durability than crystalline counterparts in the wastewater

Corresponding author: Ying-dong QU, Tel/Fax: +86-24-25497699, E-mail: quydong@sut.edu.cn;
Ke-qiang QIU, Tel/Fax: +86-24-25496031, E-mail: kqqu@sut.edu.cn

DOI: 10.1016/S1003-6326(22)65887-4

1003-6326/© 2022 The Nonferrous Metals Society of China. Published by Elsevier Ltd & Science Press

treatment. In some literatures [14,15], Mg-based amorphous ribbons have been used to treat dye wastewater. However, the research on Mg-based amorphous alloys used for pesticide wastewater treatment is scarce. QIU et al [16] found that omethoate pesticide wastewater can be degraded by the Mg-based amorphous ribbon and the chemical oxygen demand (COD) removal is 60% in 30 min, in early 2016.

The composition of an amorphous ribbon is adjustable to obtain more favorable catalytic performance. For example, $Al_{91-x}Ni_9Y_x$ [17] and $Mg_{63+x}Zn_{32-x}Ca_5$ [18] can be tuned by adjusting the contents of Y and Mg, respectively, to get high degradation efficiency for azo dye wastewater. Furthermore, the surface activity of catalysts is an essential factor in degradation reaction [19,20], so better degradation efficiency can be obtained by increasing the surface areas through changing the surface morphology for amorphous materials. Powder made by ball milling [21] and nanoporous ribbon made by dealloying [22] are two typical materials obtained by changing the surface morphology. Generally, materials in powder form usually display higher degradation efficiency due to their large specific surface area [23]. By considering the high cost of ball milling and large consumption of the powder in the solution, however, dealloying technology is used to prepare the ribbons with nanoporous structure for improving their degradation efficiency. Currently, dealloying technology mainly includes chemical dealloying and electrochemical dealloying [24,25], while amorphous ribbon has become an ideal dealloying precursor due to its homogeneous single-phase structure and homogeneity in chemical composition [26–28]. And the dealloyed ribbon with excellent catalytic performance can be used in many kinds of wastewater degradation. DENG et al [29] used Mg–Cu–Gd dealloyed ribbons to treat phenol wastewater and degradation efficiency could reach 90% after 30 min. WANG et al [30] used the Cu–Y dealloyed ribbons to treat dye wastewater and the color of the solution could be nearly faded after 30 min, showing better catalytic performance than the commercial copper foils. Besides, some Fe-based dealloyed ribbons [31,32] also show excellent catalytic performance in degrading azo dye wastewater.

Although amorphous ribbons and dealloyed

ribbons have shown great degradation efficiency in treating azo dye wastewater, few researches on the treatment of pesticide wastewater have been reported. In this work, $Mg_{65}Cu_{25-x}Ag_xY_{10}$ ($x=0, 5, 10$, at.%) dealloyed ribbons were prepared as a catalyst used to degrade pesticide wastewater. It should be noted that the amorphous ribbons prepared include some crystals in their amorphous matrix. However, the effect of galvanic cells caused by chemical inhomogeneity due to the existence of crystals is helpful to exhibit the higher reactivity for the amorphous ribbons [33], which is able to reduce the dealloying time.

2 Experimental

2.1 Preparation of ribbons

The alloy ingots with nominal compositions of $Mg_{65}Cu_{25-x}Ag_xY_{10}$ ($x=0, 5, 10$, at.%) were fabricated by induction melting a mixture of metal pieces of Mg, Cu, Ag and Y (all with a purity of 99.9 wt.% or better) under a highly purified Ar atmosphere. Then, the pieces of the ingot were put into a quartz tube to be remelted and injected onto a rotating Cu wheel for preparing the ribbons with the width of 2 mm and the thickness of about 35 μm . For simplicity, the prepared ribbons of $Mg_{65}Cu_{25}Y_{10}$, $Mg_{65}Cu_{20}Ag_5Y_{10}$ and $Mg_{65}Cu_{15}Ag_{10}Y_{10}$ are denoted as Ag_0 , Ag_5 and Ag_{10} , respectively.

The as-spun Ag_0 , Ag_5 and Ag_{10} ribbons were then immersed into dilute H_2SO_4 solution at room temperature for free corrosion until the color of the ribbons was changed to a typical Cu metallic color. Then, the dealloyed ribbons were rinsed by distilled water and alcohol before the degradation tests.

2.2 Characterization methods

The phase constituents of the as-spun and the dealloyed ribbons before and after degradation reaction were characterized by X-ray diffraction (XRD) with a $Cu K_\alpha$ radiation. The surface morphology of the dealloyed ribbons was observed by scanning electron microscope (SEM). Besides, the elemental composition of the dealloyed ribbons before and after degradation reaction was analyzed by energy-dispersive X-ray spectroscopy (EDS). The specific surface area of the dealloyed ribbons was measured by the Brunauer–Emmett–Teller (BET) method. The elemental information of the dealloyed ribbons was analyzed by X-ray

photoelectron spectroscopy (XPS). And the chemical demand oxygen (COD) was measured by fast digestion spectrophotometry.

2.3 Degradation experiments

First, to prepare the pesticide wastewater, a desirable dosage of cis-cypermethrin was mixed with the deionized water, and its desirable pH value was adjusted by concentrated H_2SO_4 . Then, the pre-weighed dosage of ribbon was put into the wastewater, which was contained in a 100 mL beaker. The degradation experiments were performed at room temperature for 90 min. During the degradation experiment, 5 mL of solution was taken out every 10 min as a sample to measure the COD value (the solution was stirred during the whole degradation process). The degradation efficiency, η , of the cis-cypermethrin wastewater can be calculated according to the following equation:

$$\eta = (C_0 - C_t) / C_0 \times 100\% \quad (1)$$

where C_0 is the initial COD of the cis-cypermethrin wastewater, and C_t is the COD at time t .

To study the influence of variables on the degradation efficiency of the wastewater, the experimental variables were set as follows: pH=1, 2, 3, 4, 7; the initial concentration of the cis-cypermethrin in the wastewater was 400, 500, 600 and 700 mg/L; the dosage of the dealloyed ribbons was 0.67, 1.33, 2.00 and 2.67 g/L.

3 Results and discussion

3.1 Microstructure of dealloyed ribbons

Figures 1(a, b) display the XRD patterns of the as-spun Ag_0 , Ag_5 , Ag_{10} ribbons and their corresponding dealloyed ribbons, respectively. In Fig. 1(a), there is a broad diffraction peak located at approximately $2\theta=38^\circ$, and some sharp crystalline diffraction peaks also appear on the XRD curves, which indicates that in the microstructure of the as-spun ribbons, there are some crystals embedded on the amorphous matrix. Compared to the as-spun ribbons, the amorphous nature for the dealloyed ribbons (Fig. 1(b)) is reduced because the intensity of the broad diffraction peaks is not so obvious, and more crystallization peaks are observed. Due to the nano-scale features of the dealloyed ribbons, they

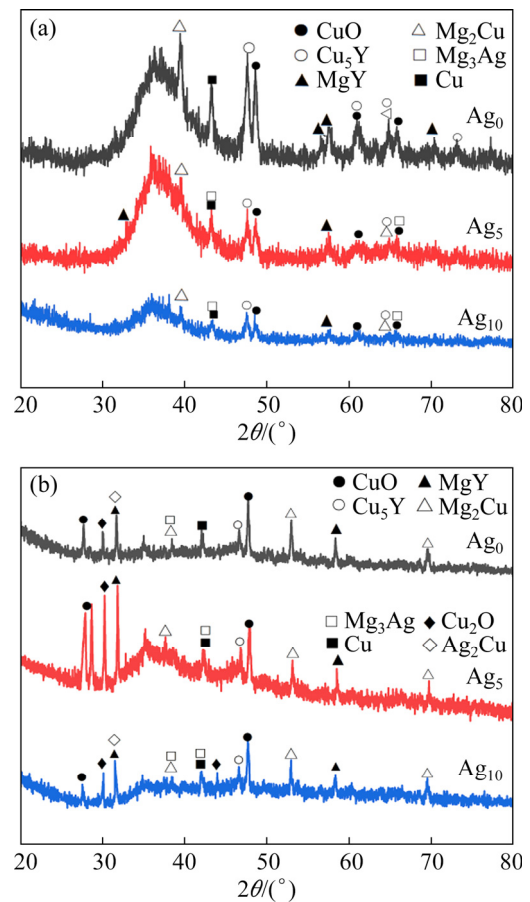


Fig. 1 XRD patterns of as-spun ribbons (a) and dealloyed ribbons (b)

may be oxidized quickly, and fresh oxidation products can be detected on their surfaces.

The surface morphologies of Ag_0 , Ag_5 , Ag_{10} dealloyed ribbons are exhibited in Figs. 2(a–c), respectively and the locally magnified SEM image of the Ag_{10} dealloyed ribbon is presented in Fig. 2(d). It is observed that the networked nanoporous structures have been formed and uniformly covered the whole surfaces of all the three dealloyed ribbons. Furthermore, with the increase of the Ag addition from 0 to 10%, the nanoporous structure becomes more and more regular, and the average sizes of nanopores for the three dealloyed ribbons are about 48.52, 70.66 and 94.48 nm, respectively, as listed in Table 1. The results indicate that the nanoporous size can be adjusted by controlling the Ag addition in the alloy composition. Compared to the ribbon with single amorphous phase, there are some crystals embedded in the amorphous matrix in the as-spun ribbon. It is well known that the existence of potential difference between the crystals and

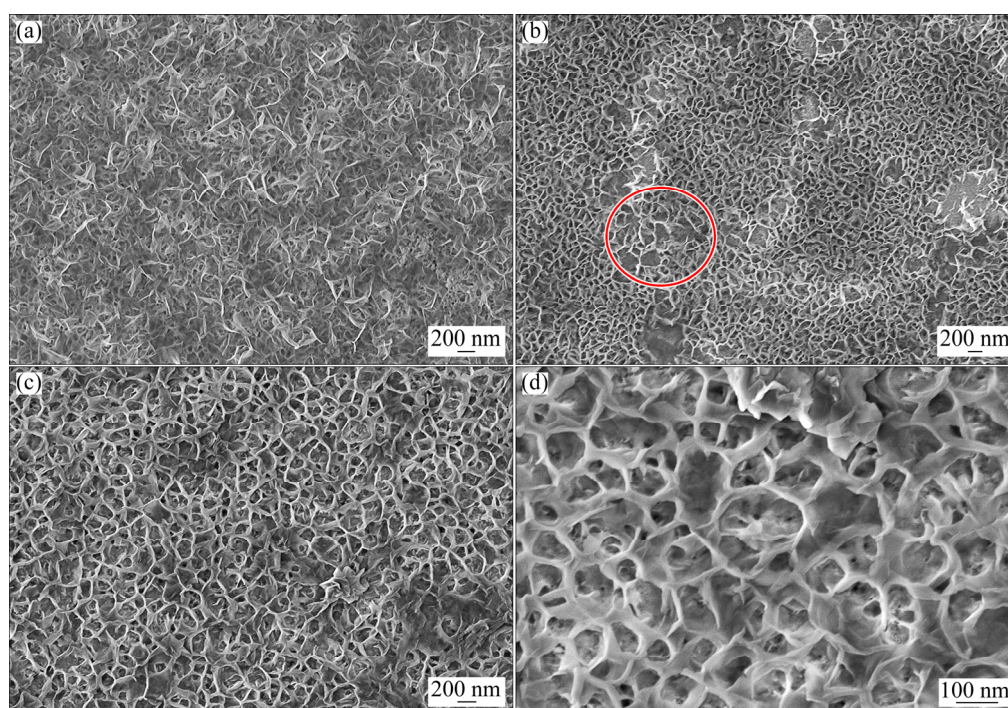


Fig. 2 SEM images of dealloyed ribbons of Ag₀ (a), Ag₅ (b), Ag₁₀ (c) and locally magnified SEM image of Ag₁₀ (d)

Table 1 Compositions and average pore size of dealloyed ribbons before degradation as well as compositions of Ag₁₀ as-spun ribbon and A₁₀ dealloyed ribbon after degradation

Sample	Element content/at.%					Average pore size/nm
	Mg	Cu	Ag	Y	O	
Ag ₀ dealloyed ribbon	47.14	25.05	–	8.07	19.74	48.52
Ag ₅ dealloyed ribbon	43.70	16.42	4.39	6.55	28.94	70.66
Ag ₁₀ dealloyed ribbon	33.58	13.42	9.36	5.98	37.66	94.48
Ag ₁₀ as-spun ribbon	62.23	14.06	10.14	9.53	4.05	–
Ag ₁₀ after degradation	3.57	22.28	15.62	4.77	53.76	–

amorphous matrix can lead to the formation of galvanic cells, which is helpful for the dealloying process. During the dealloying process, the crystals with lower corrosion potential in the ribbon is preferentially dissolved, and the crystals with higher corrosion potential is subsequently dissolved to form a part of pores [34,35]. As shown in Fig. 2(b), some larger pores or defect areas are irregularly distributed on the surface, as indicated by a red circle, corresponding to the crystals

embedded in the amorphous matrix. The other pores mainly come from the dissolution and reorganization of the elements in the amorphous matrix [34,36]. The average compositions of the dealloyed ribbons are listed in Table 1. The dealloying process mainly consumes Mg in the ribbon, while most of Cu and Ag remained in the dealloyed ribbon can diffuse and recombine to form the ligament of networked nanoporous structure. It is further found from Table 1 that Mg content is significantly reduced after dealloying due to the increase of Ag content, which enlarges the potential difference between Ag and Mg elements [37], resulting in the increase of Mg dissolution and therefore a large pore size. Since the dealloying time of the ribbon is controlled in a limited period, the dealloyed ribbons contain all elements as the original as-spun ones, implying that the as-spun ribbons are merely partially dealloyed. In fact, only a layer of nanoporous structure of about $\sim 0.6 \mu\text{m}$ is formed, as indicated by Fig. 3. Compared to the surface morphology shown in Fig. 2(c) for the same sample, it is found that the size of the nanoporous structure on the cross-section is relatively smaller.

3.2 Degradation properties

Figure 4 shows the influence of Ag addition on the degradation efficiency and degradation rate of

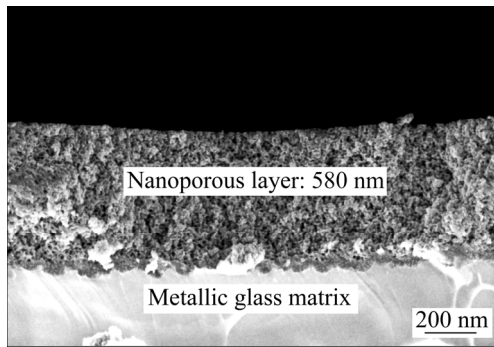


Fig. 3 SEM image of cross-section of Ag₁₀ dealloyed ribbon

the wastewater. The degradation experiments were carried out with such parameters as the pH value of 3, the initial cis-cypermethrin concentration of 500 mg/L, and the dealloyed ribbon dosage of 1.33 g/L. The results indicate that the degradation efficiency of the wastewater increases gradually with increasing the Ag addition. When the Ag addition increases from 0 to 5% and further to 10%, the degradation efficiency is increased from 90% to 93% and to 95.8%. Meanwhile, the value of the degradation rate constant k is obviously increased from 0.03856 to 0.05002 (Fig. 4(b)). The pore sizes of the dealloyed ribbons can explain these results. From Table 1 and Fig. 2, it can be seen that the pore sizes increase with Ag addition. Obviously, the Ag₁₀ dealloyed ribbon with a larger pore size and more Ag content displays better degradation capacity than the other two dealloyed ribbons. The similar results can be found for the Mg–Cu–Gd dealloyed ribbon [29]. From Fig. 4(a), the degradation efficiency can nearly reach the maximum within 60 min. A linear relationship between $\ln(C_0/C_t)$ and t implies that the degradation process conforms to the first order reaction kinetics model. The degradation rate constant k can be calculated according to the following equation [38]:

$$\ln(C_0/C_t) = kt \quad (2)$$

Since the Ag₁₀ dealloyed ribbon exhibits the highest degradation efficiency, the results discussed in the following sections are all focused on the Ag₁₀ dealloyed ribbon.

In order to compare the dealloying effect, the degradation efficiency of the as-spun and dealloyed ribbons of the Ag₁₀ alloy was investigated under the

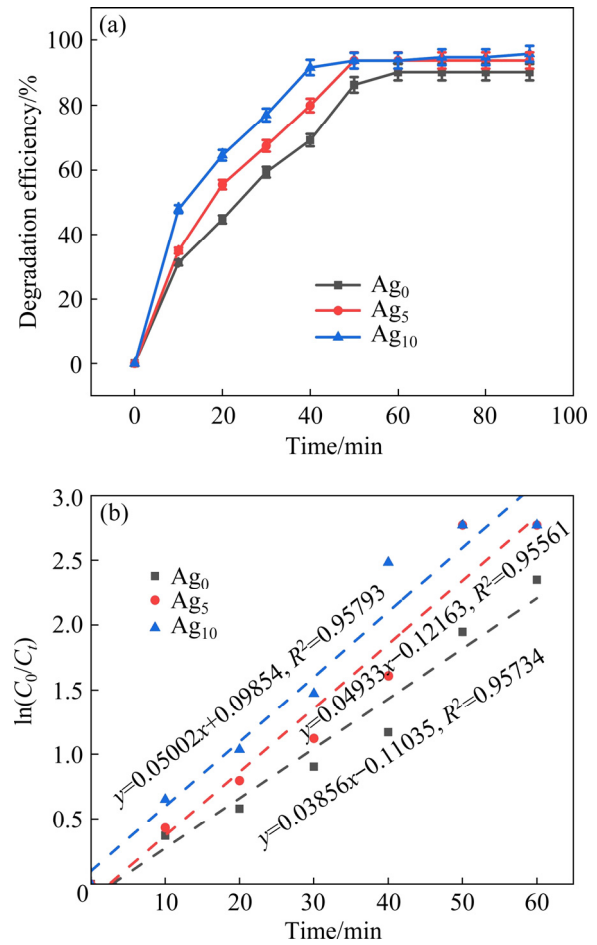


Fig. 4 Effect of Ag addition in dealloyed ribbon on degradation efficiency (a) and rate constant (b)

same conditions as above by considering the difference between their specific surface areas. The specific surface area of two kinds of ribbons was measured based on the BET method. The specific surface area of the dealloyed ribbons is 2.814986 m²/g, which is more than 100 times larger than that of the as-spun ribbons (0.026492 m²/g). Figure 5 shows the influence of specific surface area on the degradation efficiency of wastewater. The degradation efficiency of the as-spun ribbon is nearly 60% after 90 min, while it is nearly 40% after only 10 min and reaches 90% after 40 min for the dealloyed ribbon. Therefore, the specific surface area plays an essential role in increasing the degradation efficiency by increasing the active sites. In addition, the degradation experiments of Ag₁₀ pure amorphous ribbon were also carried out and the largest degradation efficiency of about 70% was obtained under the same conditions, as shown in Fig. 5. Although the degradation efficiency of the pure amorphous ribbons is better than that of the

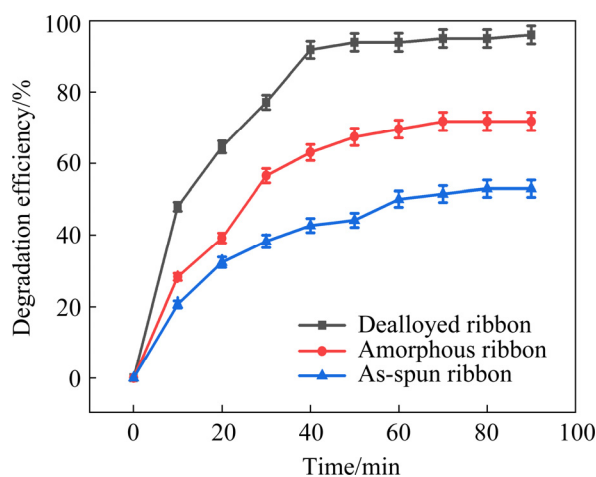


Fig. 5 Effect of specific surface area of Ag_{10} ribbons on degradation efficiency of cis-cypermethrin wastewater

as-spun ribbons, it is still lower than that of the dealloyed ribbons, which further indicates that the specific surface area plays an important role in the degradation process.

In order to consider the effect of pH on the degradation process, the degradation experiments at different pH values of 1, 2, 3, 4 and 7 were carried out under the conditions of pesticide concentration being 500 mg/L and dealloyed ribbon dosage being 1.33 g/L. In Fig. 6(a), it is obvious that the degradation efficiency for wastewater with pH=3 is the largest at any processing time. At pH=3, the degradation efficiency reaches approximately 40% in the first 10 min and approaches to the maximum in less than 60 min. Accordingly, the degradation rate is more than 2 times larger than that of others (Fig. 6(b)). Furthermore, when the pH value is either increased or decreased, the degradation efficiency is unavoidably dropped. When the pH value is less than 3, the H^+ concentration is so high that the H^+ will destroy the nanoporous structure of the dealloyed ribbon. Besides, excessive $[\text{H}^+]$ will synthesize and generate H_2 quickly, which will be absorbed and occupy the active sites of nanopores, so that the degradation efficiency will decrease. If the pH value is high, the concentration of H^+ cannot form enough $[\text{H}^+]$ for degradation.

The dependence of the degradation efficiency on the initial concentration of cis-cypermethrin in the wastewater is presented in Fig. 7(a), and the other experimental conditions were kept at the pH of 3 and the ribbon dosage of 1.33 g/L. From Fig. 7(a), it is observed that when the initial

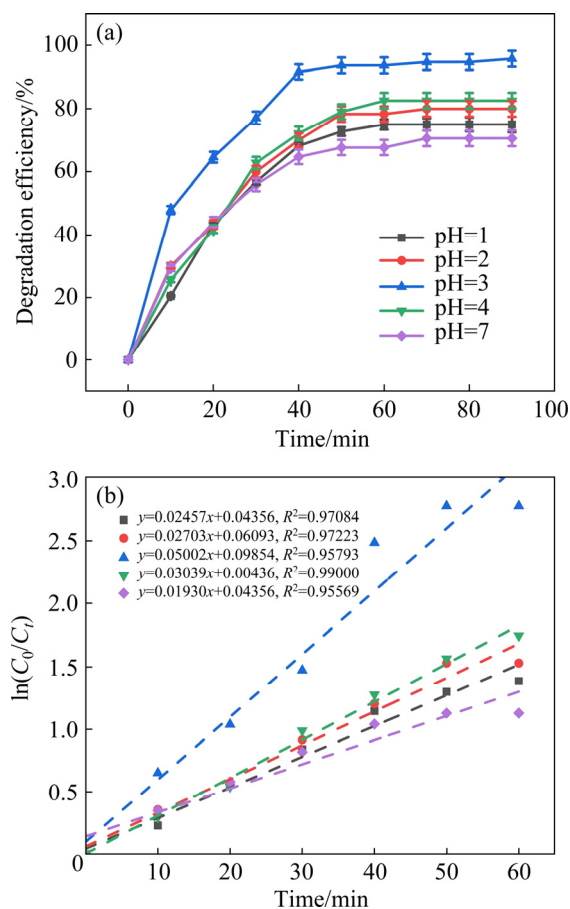


Fig. 6 Effect of pH on degradation efficiency (a) and degradation rate constant (b)

concentration of the cis-cypermethrin in the wastewater is 500 mg/L, the degradation efficiency is larger than that with other initial concentrations. With decreasing initial cypermethrin concentration from 500 to 400 mg/L, the degradation efficiency is decreased from 95.8% to 88%; while increasing the initial cis-cypermethrin concentration to 600 or to 700 mg/L, the degradation efficiency is further reduced. The degradation rate constant presents the same change tendency as the degradation efficiency varying with the initial pesticide concentrations (Fig. 7(b)). Therefore, optimal initial concentration of cis-cypermethrin is 500 mg/L.

The ribbon dosage is another vital factor affecting the degradation efficiency and rate of the cis-cypermethrin wastewater and the results are shown in Figs. 7(c, d) respectively, under the existing optimal experimental conditions of the pH being 3 and the initial cis-cypermethrin concentration being 500 mg/L. It is seen that with the increase of the dealloyed ribbon dosage from 0.67 to 1.33 g/L, the degradation efficiency

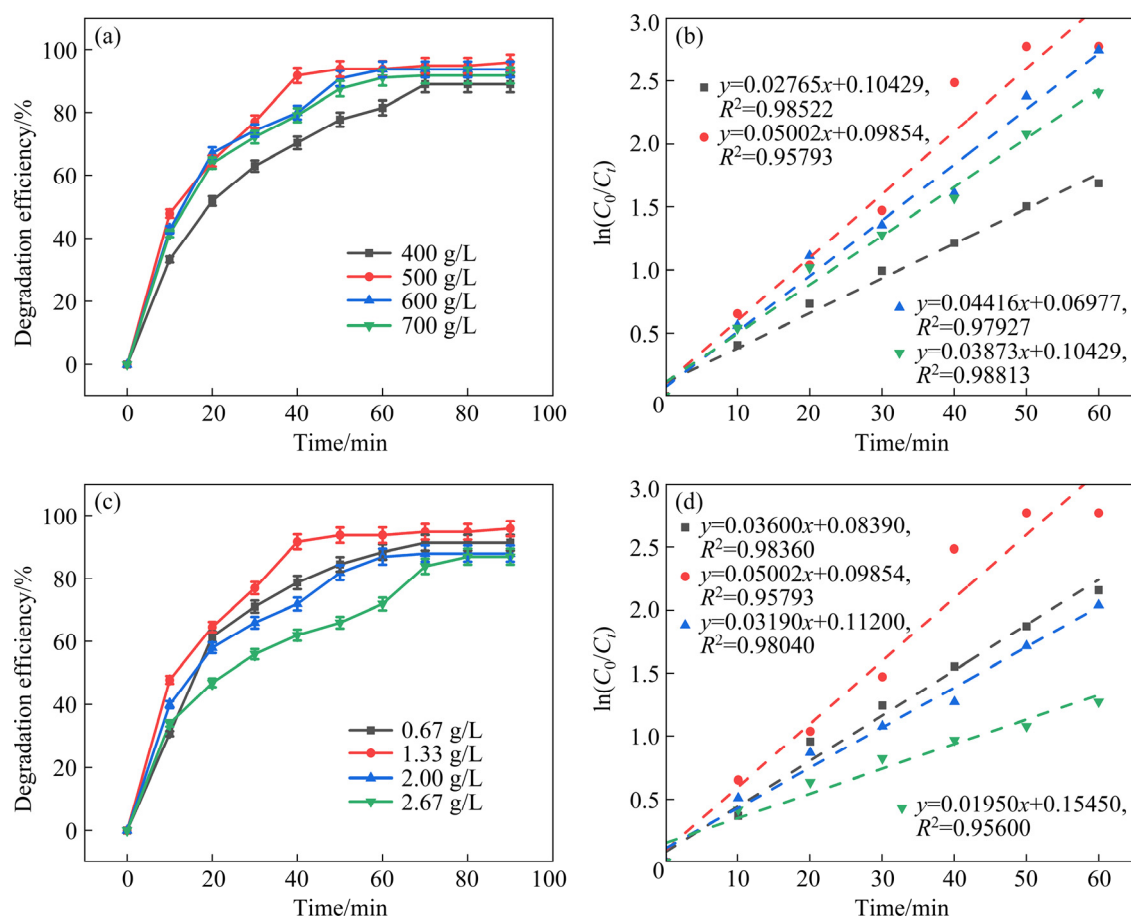


Fig. 7 Effect of initial concentration of cis-cypermethrin on degradation efficiency (a) and degradation rate constant (b) of wastewater by using Ag₁₀ dealloyed ribbon with dosage of 1.33 g/L, and effect of dosage of dealloyed ribbon on degradation efficiency (c) and degradation rate constant (d) for wastewater with initial cis-cypermethrin concentration of 500 mg/L

increases from 81% to 95.8%. However, with further increase of the dealloyed ribbon dosage to 2.00 and further to 2.67 g/L, the degradation efficiency is decreased to 88% and to 87%, respectively. The above results indicate that the suitable ribbon dosage under these experimental conditions should be 1.33 g/L.

The same principle can explain the change in the degradation efficiency of these two factors. When the dosage of ribbons is constant, the number of active sites is also constant. If the cis-cypermethrin concentration is lower, the number of active sites is more than that needed for the contaminant molecules and the active sites do not fully take the function. Therefore, as the cis-cypermethrin concentration increases, the degradation efficiency increases obviously. However, if the cis-cypermethrin concentration is further increased, the ribbons cannot provide enough active sites to degrade it. Similarly, when

the initial cis-cypermethrin concentration is constant, the appropriate dosage of ribbons is also required. In this experiment, therefore, the optimal cis-cypermethrin concentration and the optimal dosage of ribbon are 500 mg/L and 1.33 g/L, respectively, which indicates that the number of active sites and pesticide molecules should be matched in order to get a high degradation efficiency for the wastewater.

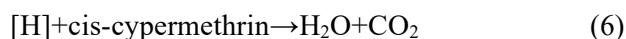
3.3 Degradation mechanism

According to the degradation experiments mentioned above, the dealloyed ribbons exhibit an excellent catalytic performance in the degradation process. In order to understand the possible mechanism of degradation, the experimental phenomena are summarized first.

Whenever the dealloyed ribbon was put into the beaker containing the cis-cypermethrin wastewater, many fine bubbles were produced and

floated onto the surface of the solution. With increasing the degradation time, the number of bubbles was decreased. It was shown that the measured pH value of the solution was increased from 3 to near neutral. Then, a large number of fine precipitations were floated in the wastewater, and the precipitations were gradually increased and settled to the bottom of the beaker. At the end of the degradation experiments, the cis-cypermethrin wastewater became clear.

The degradation process is mainly divided into two processes: adsorption and catalysis [39]. Firstly, a large number of pesticide molecules are absorbed on the surface of the dealloyed ribbon and involved in the subsequent catalytic reaction. Two kinds of catalytic reactions take place. One is that the pesticide molecules catch electrons directly from the surface of the dealloyed ribbon when they collide with the ribbon, while the other is that the pesticide molecules are catalyzed by reducing species [40]. The formation of reducing species, i.e., the reducing hydrogen here, is as follows: the metal atom such as Mg in the dealloyed ribbons releases electrons [41], and the H^+ in the solution combines with the released electron to generate $[H]$, which is a strong reducing species with high reactivity so that it can degrade the pesticide wastewater to H_2O and CO_2 . Meanwhile, the galvanic cell formed between the nanoporous layer and amorphous matrix also helps for increasing the transfer rate of electrons in the wastewater, accelerating its degradation rate [33,42]. The degradation reaction of the pesticide wastewater can be listed as follows [42,43]:



where M is metal atoms that lose electrons during the reaction; n is the number of electrons transferred; e denotes electron. It should be mentioned that the nanoporous structure of the dealloyed ribbon provides excellent interconnected channels, which can accelerate the transport of molecules and electrons, so the degradation reaction becomes faster.

According to the Reactions (3)–(5), the fine bubbles produced in the degradation process are H_2

gas bubbles, which prove that the catalytic reaction takes place. Since $[H]$ mainly depends on the H^+ in the solution, the dealloyed ribbon demonstrates excellent catalytic performance in acidic solution. When the pH value becomes neutral, the catalytic reaction becomes weak gradually, so the number of bubbles is decreased. The nanoporous structure on the surface of the ribbon can provide a strong absorptivity to quickly adsorb the pesticide molecules to the surface of the ribbons to improve the catalytic reactions. Meanwhile, there are a large number of atomic steps on the outer surface of the nanoporous structure [44], which can provide enough energy to easily break the bonds of macromolecules [45,46]. Therefore, the pesticide molecules are degraded.

In order to further investigate the degradation mechanism of the pesticide, the surface morphologies and the elements of the dealloyed ribbons after the reaction were analyzed, and the corresponding results are presented in Fig. 8 and Table 1, respectively. The general morphology of the dealloyed ribbon after degradation is shown in Fig. 8(a). Without surprise, a flat surface without nanoporous structure is observed. Figures 8(b, c) display the magnified images of the flat reaction region (indicated by a yellow square in Fig. 8(a)) and the pit reaction region (indicated by a red square in Fig. 8(a)), respectively. It is seen that many by-products are littered in the flat reaction region (Fig. 8(b)), while in the pit region, it shows the more serious cotton-like corrosion morphology (Fig. 8(c)).

In addition, the change of the elements in the dealloyed ribbon is also notable. After catalytic degradation, the elements are detected mainly as Cu, Ag, Y and O on the ribbon surface as shown in Figs. 8(d, e). Compared to the dealloyed ribbon before catalytic degradation, the production of a large amount of O element on the surface after degradation proves the formation of oxidation products. Therefore, the production of oxides can act as one of the possible evidences for catalytic degradation. According to the above discussion, the higher content of O element in the pit region indicates that the catalytic degradation in pit is intenser than that in the flat reaction region. The reason for this phenomenon is that the pit provides more active sites available during the reaction. After the reaction, the Mg content on the surface of the

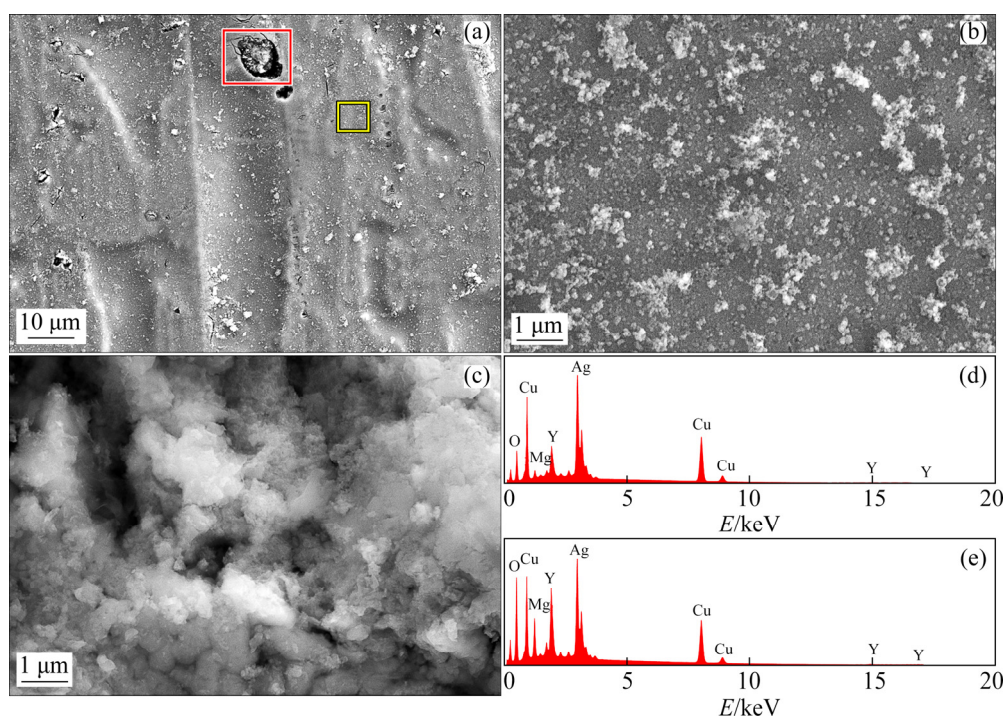


Fig. 8 SEM image of Ag₁₀ dealloyed ribbon after degradation reaction (a); magnified SEM images of flat region (b) and concave region (c) on dealloyed ribbon; EDS analysis results of flat (d) and concave (e) regions on dealloyed ribbon

ribbon decreases sharply, which means that there is a large amount of Mg²⁺ in the solution during the degradation process, and such a large amount of Mg²⁺ will undergo hydrolysis to form Mg(OH)₂ through co-precipitation to affect the degradation reaction. Mg(OH)₂ is able to adsorb pesticide molecules effectively due to its large specific surface area to affect the degradation reaction. Subsequently, these insoluble substances will sink to the bottom of the beaker, so a large number of precipitations can be observed on the bottom of the beaker after the degradation tests.

The chemical condition about the surface of the dealloyed ribbon can be further analyzed by XPS, and the spectra before and after degradation are shown in Fig. 9. For the dealloyed ribbon after degradation, as shown in Fig. 9(a), the Cu 2p peaks are located at 932.7 and 933.8 eV with two satellite peaks which can be determined as Cu⁺ and Cu²⁺ [47]. As seen in Fig. 9(b), the peaks from O 1s can be divided into three types of bonds, i.e., MO, OH⁻ and absorbed O bonds. Combined with O 1s spectra (Fig. 9(b)), Cu⁺ and Cu²⁺ are assigned to Cu₂O, CuO and Cu(OH)₂, respectively [47,48]. In Figs. 9(c, d), the Mg²⁺ and Y³⁺ mainly exist in the form of MgO (1303.9 eV) and Y₂O₃ (157.9 eV, 160.2 eV) [49]. The reason why Mg(OH)₂ is not

observed is that it participates in the adsorption reaction immediately after it is produced in the solution, and then is precipitated to the bottom of the beaker. It is worth noting that the Cu₂O produced can directly reduce the pesticide molecules due to its strong reducing performance. Combined with the spectra in Figs. 9(a, b, d) before reaction, it is interpreted that Cu⁰ (932.6 eV) and Y⁰ (156.4 eV) on the surface of the dealloyed ribbon are converted to Cu⁺ (Cu₂O), Cu²⁺ (CuO) and Y³⁺ (Y₂O₃) after degradation. From Fig. 9(c), the surface of the dealloyed ribbon before degradation is mainly covered by MgO and MgSO₄, while Mg on the surface of the ribbon after reaction only exists in the form of MgO. These phenomena indicate that the oxidation products can be formed in the process of degradation reaction and the electrons transfer is beneficial to the degradation reaction.

The XPS results further confirm that the surface of the dealloyed ribbon after the reaction is mainly covered by the oxidation products and hydroxides. Therefore, the contact between the ribbon and the cis-cypermethrin molecules is prevented at a later stage of degradation, which causes the catalyzed process to cease and the degradation efficiency to decrease. Thus, it can be inferred that adsorption is a significant process for

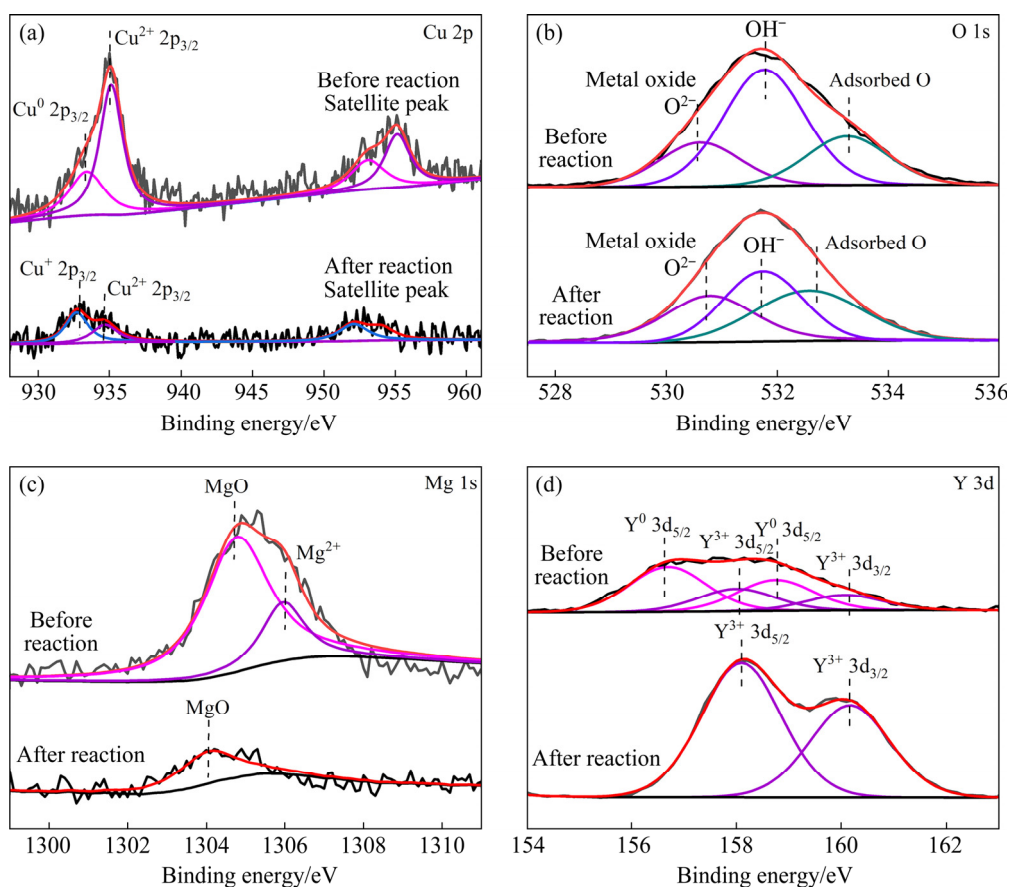


Fig. 9 XPS spectra of Ag_{10} dealloyed ribbons before and after degradation: (a) Cu 2p; (b) O 1s; (c) Mg 1s; (d) Y 3d

the cis-cypermethrin degradation. Fortunately, the uniformly distributed nanopores on the dealloyed ribbon surface can provide a larger area and more catalytic active sites, which is beneficial to the adsorption and catalytic reaction, so such a higher degradation efficiency can be obtained. Meanwhile, an assistant role presented by the galvanic cells further accelerates the transfer of electrons. From the results, the cis-cypermethrin is mineralized, and the by-products are non-toxic and harmless, which will not cause secondary pollution to the environment. According to the mechanism mentioned above, the schematic diagram of pesticide degradation by the dealloyed ribbon is presented in Fig. 10.

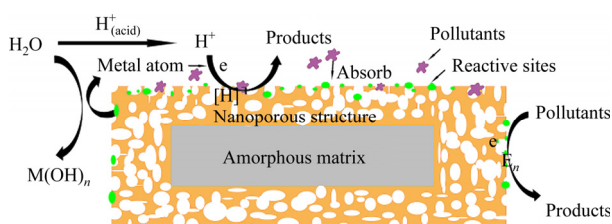


Fig. 10 Schematic diagram of pesticide degradation by dealloyed ribbon

4 Conclusions

(1) The networked nanoporous structures with the average pore sizes of 46.3, 70.4, and 94.4 nm are developed by dealloying the as-spun ribbons of $\text{Mg}_{65}\text{Cu}_{25}\text{Y}_{10}$, $\text{Mg}_{65}\text{Cu}_{20}\text{Ag}_5\text{Y}_{10}$, $\text{Mg}_{65}\text{Cu}_{15}\text{Ag}_{10}\text{Y}_{10}$, respectively, and both the pore size and degradation efficiency are obviously increased with increasing the Ag addition.

(2) The optimal degradation parameters, i.e., pH 3, the initial cis-cypermethrin concentration of 500 mg/L, and the dealloyed ribbon dosage of 1.33 g/L, are obtained at ambient temperature, and the maximum degradation efficiency of the pesticide wastewater is as large as 95.8%.

(3) The degradation mechanism includes two kinds of processes: one is the adsorption process and the other is the catalytic reaction. The dealloyed ribbon with many nanoscale pores and large specific surface area makes the adsorption process easier. The catalytic reaction is more complex, which includes dehydrogenation, reduction, oxidation as well as the effect of galvanic cells.

Acknowledgments

The authors are grateful for the financial supports from State Key Laboratory of Light Alloy Casting Technology for High-end Equipment, the Natural Science Foundation of Liaoning Province, China (No. 2020-KF-14-03), and the National Natural Science Foundation of China (No. 51775353).

References

- [1] PARVEEN S, BHATTI I, ASHAR A, JAVED T, MOHSIN M, HUSSAIN M T, KHAN M I, NAZ S, IQBAL M. Synthesis characterization and photocatalytic performance of iron molybdate ($\text{Fe}_2(\text{MoO}_4)_3$) for the degradation of endosulfan pesticide [J]. *Materials Research Express*, 2020, 7: 035016.
- [2] HUO Qiang, LIU Xi, CHEN Li-jun, WU Yong-hong, WU Hai-yan, XIE Jian-ping, LIU Xin-xing, QIU Guan-zhou. Treatment of backwater in bauxite flotation plant and optimization by using Box-Behnken design [J]. *Transactions of Nonferrous Metals Society of China*, 2019, 29: 821–830.
- [3] HITKARI G, SINGH S, PANDEY G. Photoluminescence behavior and visible light photocatalytic activity of ZnO , ZnO/ZnS and $\text{ZnO/ZnS}/\alpha\text{-Fe}_2\text{O}_3$ nanocomposites [J]. *Transactions of Nonferrous Metals Society of China*, 2018, 28: 1386–1396.
- [4] ZHAO Guo-qing, ZHENG Yi-jian, HE Zhi-guo, LU Ze-xiang, WANG Long, LI Cai-feng, JIAO Fei-peng, DENG Chun-yan. Synthesis of Bi_2S_3 microsphere and its efficient photocatalytic activity under visible-light irradiation [J]. *Transactions of Nonferrous Metals Society of China*, 2018, 28: 2002–2010.
- [5] ZHAO Wen-hua, WEI Zhi-qing, WU Xiao-juan, ZHANG Xu-dong, ZHANG Li, WANG Xuan. Microstructure and photocatalytic activity of Ni-doped ZnS nanorods prepared by hydrothermal method [J]. *Transactions of Nonferrous Metals Society of China*, 2019, 29: 157–164.
- [6] WANG Yan, FAN Cai-mei, HUA Bo, LIANG Zhen-hai, SUN Yan-pin. Photoelectrocatalytic activity of two antimony doped SnO_2 films for oxidation of phenol pollutants [J]. *Transactions of Nonferrous Metals Society of China*, 2009, 19: 778–783.
- [7] CONG Lu-jing, GUO Jing, LIU Ji-song, SHI Hai-yan, WANG Ming-hua. Rapid degradation of endosulfan by zero-valent zinc in water and soil [J]. *Journal Environmental Management*, 2015, 150: 415–455.
- [8] KOPINKE F D, SUHNHOLZ S, GEORGI A, MACKENZIE K. Interaction of zero-valent iron and carbonaceous materials for reduction of DDT [J]. *Chemosphere*, 2020, 253: 126712.
- [9] MAI A, HADNAGY E, ABRAHAM J, TERRACCIANO A, ZHENG Z, SMOLINSKI B, KOUTSOSPYROS A, CHRISTODOULATOS C. Determining degradation kinetics, byproducts and toxicity for the reductive treatment of Nitroguanidine (NQ) by magnesium-based bimetal Mg/Cu [J]. *Journal of Hazardous Materials*, 2022, 423: 126943.
- [10] SICILIANO A, CURCIO G M, LIMONTI C. Hexavalent chromium reduction by zero-valent magnesium particles in column systems [J]. *Journal of Environmental Management*, 2021, 293: 112905.
- [11] WANG Jun-qiang, LIU Yan-hui, CHEN Ming-wei, LOUZGUINE L D V, INOUE A, PEREPEZKO J H. Excellent capability in degrading azo dyes by MgZn-based metallic glass powders [J]. *Scientific Reports*, 2012, 2: 418.
- [12] ZHANG Chang-qin, ZHU Zheng-wang, ZHANG Hai-feng, HU Zhuang-qi. Rapid reductive degradation of azo dyes by a unique structure of amorphous alloys [J]. *Chinese Science Bulletin*, 2011, 56: 3988–3992.
- [13] WANG Jun-qiang, LIU Yan-hui, CHEN Ming-wei, XIE Guo-qiang, DMITRI V, LOUNGUINE L, AKIHISA I, JOHN H P. Rapid degradation of azo dye by Fe-based metallic glass powder [J]. *Advanced Functional Materials*, 2012, 22: 2567–2570.
- [14] IQBAL M, WANG W H. Synthesis and characterization of Mg-based amorphous alloys and their use for decolorization of azo dyes [J]. *IOP Conference Series: Materials Science and Engineering*, 2014, 60: 012035.
- [15] CHEN Peng, HU Xi-mei, QI Yu-min, WANG Xin, LI Zhong-jia, ZHAO Li-chen, LIU Shui-qing, CUI Chun-xiang. Rapid degradation of azo dyes by melt-spun Mg–Zn–Ca metallic glass in artificial seawater [J]. *Metals-Open Access Metallurgy Journal*, 2017, 7: 485.
- [16] QIU Ke-qiang, WANG Ting-feng, YUE Chun-yu, REN Ying-lei. Degradation effect of $\text{Mg}_{75}\text{Zn}_{20}\text{Ca}_5$ amorphous ribbon on omethoate pesticide wastewater [J]. *Journal of Shenyang University of Technology*, 2016, 38: 268–273. (in Chinese)
- [17] WANG Pei-pei, WANG Jun-qiang, LI He, YANG Hao, HUO Jun-tao, WANG Jian-guo, CHANG Chun-tao, WANG Xin-min, LI Run-wei, WANG Gang. Fast decolorization of azo dyes in both alkaline and acidic solutions by Al-based metallic glasses [J]. *Journal of Alloy and Compounds*, 2017, 701: 759–767.
- [18] ZHAO Y F, SI J J, SONG J G, YANG Q, HUI X D. Synthesis of Mg–Zn–Ca metallic glasses by gas-atomization and their excellent capability in degrading azo dyes [J]. *Materials Science and Engineering B–Advanced Functional Solid-State Materials*, 2014, 181: 46–55.
- [19] GOTPAGAR J, LYUKSYUTOV S, COHN R, GRULKE E, BHATTACHARYYA D. Reductive dehalogenation of trichloroethylene with zero-valent iron: Surface profiling microscopy and rate enhancement studies [J]. *Langmuir*, 1999, 15: 8412–8420.
- [20] RUIZ N, SEAL S, REINHART D. Surface chemical reactivity in selected zero-valent iron samples used in groundwater remediation [J]. *Journal of Hazard Materials*, 2000, 80: 107–117.
- [21] ISLAM M A, AHSAN M Z, SATTER S S, BALLY M A A, KHAN F A. Structural and magnetic properties of ball-milled powders of $(\text{Fe}_{1-x}\text{Mn}_x)_{75}\text{P}_{15}\text{C}_{10}$ metal-glass [J]. *Aip Advances*, 2021, 11: 025036.
- [22] LUO Xue-kun, LI Ran, HUANG Lu, ZHANG Tao. Nucleation and growth of nanoporous copper ligaments during electrochemical dealloying of Mg-based metallic glasses [J]. *Corrosion Science*, 2013, 67: 100–108.
- [23] XIE Sheng-hui, PENG Guang-qiang, TU Xian-meng, QIAN

- Hai-xia, ZENG Xie-rong. Fe-based powders prepared by ball-milling with considerable degradation efficiency to methyl orange compared with Fe-based metallic glasses [J]. *Acta Metallurgica Sinica (English Letters)*, 2018, 31: 1207–1214.
- [24] LIU Xin-yi, WANG Ying-min, QIANG Jian-bing, WANG Bao-lin, MA Dian-guo, ZHANG Wei, DONG Chuang. Preparation and electro-catalytic activity of nanoporous palladium by dealloying rapidly-quenched Al₇₀Pd₁₇Fe₁₃ quasicrystalline alloy [J]. *Transactions of Nonferrous Metals Society of China*, 2019, 29: 785–790.
- [25] LI Jie, YU Na-na, JIANG Hua-wei, LENG JIN-feng, GENG Hao-ran. Effects of annealing temperature on dealloying of Ti–Cu Alloy [J]. *Corrosion Science*, 2015, 91: 95–100.
- [26] DAN Zhen-hua, QIN Feng-xiang, YAMAURA S I, XIE Guo-qiang, MAKINO A, HARA N. Refinement of nanoporous copper by dealloying MgCuY amorphous alloys in sulfuric acids containing polyvinylpyrrolidone [J]. *Journal of the Electrochemical Society*, 2014, 161: C120–C125.
- [27] JIN Yu, LI Ran, ZUO Lei, ZHANG Tao. Correlation between dealloying conditions and coarsening behaviors of nanoporous silver produced by chemical dealloying of Ca–Ag metallic glass [J]. *Journal of Alloys and Compounds*, 2017, 695: 1600–1609.
- [28] LUO Xue-kun, LI Ran, LIU Zeng-qian, HUANG Lu, SHI Min-jie, XU Tao, ZHANG Tao. Three-dimensional nanoporous copper with high surface area by dealloying Mg–Cu–Y metallic glasses [J]. *Materials Letters*, 2012, 76: 96–99.
- [29] DENG Zhen, ZHANG Cheng, LIU Lin. Chemically dealloyed MgCuGd metallic glass with enhanced catalytic activity in degradation of phenol [J]. *Intermetallics*, 2014, 52: 9–14.
- [30] WANG Ning, PAN Ye, WU Shi-kai, ZHANG En-ming, DAI Wei-ji. Fabrication of nanoporous copper with tunable ligaments and promising sonocatalytic performance by dealloying Cu–Y metallic glasses [J]. *RSC Advances*, 2017, 7: 43255–43265.
- [31] LIANG Shun-xing, ZHANG Wen-chang, WANG Wei-min, JIA Guo-hua, YANG Wei-ming, ZHANG Lai-Chang. Surface reactivation of FeNiPC metallic glass: A strategy for highly enhanced catalytic behavior [J]. *Journal of Physics and Chemistry of Solids*, 2019, 132: 89–98.
- [32] WANG J C, LIANG S X, JIA Z, ZHANG W C, WANG W M, LIU Y Z, LU J, ZHANG L C. Chemically dealloyed Fe-based metallic glass with void channels-like architecture for highly enhanced peroxymonosulfate activation in catalysis [J]. *Journal of Alloys and Compounds*, 2019, 785: 642–650.
- [33] CHEN Shuang-qin, HUI Ke-zhen, DONG Liang-zheng, LI Zhun, ZHANG Qing-hua, GU Lin, ZHAO Wei, LAN Si, KE Yu-bin, SHAO Yang, HAHN H, YAO Ke-fu. Excellent long-term reactivity of inhomogeneous nanoscale Fe-based metallic glass in wastewater purification [J]. *Science China–Materials*, 2020, 63: 453–466.
- [34] LI R, LIU X J, WANG H, WU Y, CHU X M, LU Z P. Nanoporous silver with tunable pore characteristics and superior surface enhanced Raman scattering [J]. *Corrosion Science*, 2014, 84: 159–164.
- [35] WENG Nan, WANG Feng, QIN Feng-xiang, TANG Wan-ying, DAN Zhen-hua. Enhanced azo-dyes degradation performance of Fe–Si–B–P nanoporous architecture [J]. *Materials*, 2017, 10: 1001.
- [36] ABURADA T, FITZ G J M, SCULLY J R. Synthesis of nanoporous copper by dealloying of Al–Cu–Mg amorphous alloys in acidic solution: The effect of nickel [J]. *Corrosion Science*, 2011, 53: 1627–1632.
- [37] ZHOU Yang. Fabrication of Nanoporous cobalt and its catalytic degradation of azo dyes [D]. Nanjing: Nanjing University of Science and Technology, 2018: 1–57. (in Chinese)
- [38] ZHU Shan-shan, XIANG Qing-chun, MA Chun-yan, REN Ying-lei, QIU Ke-qiang. Continuous electrocoagulation degradation of oily wastewater with Fe₇₈Si₉B₁₃ amorphous ribbons [J]. *Environmental Science and Pollution Research*, 2020, 27: 40101–40108.
- [39] DONG Chang-sheng, ZHONG Min-lin, HUANG Ting, MA Ming-xing, WORTMANN D, WORTMANN D, BRAJDIC M, KELBASSA I. Photodegradation of methyl orange under visible light by micro-nano hierarchical Cu₂O structure fabricated by hybrid laser processing and chemical dealloying [J]. *Acs Applied Materials and Interfaces*, 2011, 3: 4332–4338.
- [40] ZHAO Bo-wen, ZHU Zheng-wang, QIN Xin-dong, LI Zheng-kun, ZHANG Hai-feng. Highly efficient and stable CuZr-based metallic glassy catalysts for azo dye degradation [J]. *Materials Science and Technology*, 2020, 46: 88–97.
- [41] ZHANG Chang-qin, ZHU Zheng-wang, ZHANG Hai-feng. Mg-based amorphous alloys for decolorization of azo dyes [J]. *Results in Physics*, 2017, 7: 2054–2056.
- [42] LUO Xue-kun, LI Ran, ZONG Jing-zhen, ZHANG Ying, LI Hai-feng, ZHANG Tao. Enhanced degradation of azo dye by nanoporous-copper-decorated Mg–Cu–Y metallic glass powder through dealloying pretreatment [J]. *Applied Surface Science*, 2014, 305: 314–320.
- [43] ABOLIGHASEMABADI M, MBAREK W B, CASABELLIA O, ROCA B H, PINEDA E, ESCODA L, SUNOL J J. Application of mechanically alloyed MnAl particles to de-colorization of azo dyes [J]. *Journal of Alloys and Compounds*, 2018, 741: 240–245.
- [44] WANG Shu-shen, LIN Lin. Fabrication of novel nanoporous copper powder catalyst by dealloying of ZrCuNiAl amorphous powders for the application of wastewater treatments [J]. *Journal of Hazardous Materials*, 2017, 340: 445–453.
- [45] GERALD D M, MICHEL B. Classical kinetic of catalytic reaction [J]. *Cheminform*, 2003, 216: 89–97.
- [46] YANG Jian-fei, BIAN, Xiu-fang, BAI Yan-wen, LV Xiao-qian, WANG Pan. Rapid organism degradation function of Fe-based alloys in high concentration wastewater [J]. *Journal of Non-Crystalline Solids*, 2012, 358, 2571–2574.
- [47] QIN Chun-ling, ZHANG Meng-meng, LI Bao-e, LI Yong-yan, WANG Zhi-feng. Ag particles modified Cu₂O (x=1, 2) nanowires on nanoporous Cu–Ag bimetal network for antibacterial applications [J]. *Materials Letters*, 2020, 258: 126823.
- [48] WANG Qian-qian, YUN Lu, CHEN Ming-xiu, XU Dan-dan,

CUI Zhi-qiang, ZENG Qiao-shi, LI Ping-hua, CHU Cheng-lin, SHEN Bao-long. Competitive effect of structural heterogeneity and surface chemical states on catalytic efficiency of FeSiBPCu amorphous and nanocrystalline alloys [J]. ACS Applied Nano Materials, 2019, 2: 214–227.

[49] YANG Xue, XU Xiao-chen, XIANG Qing-chun, QU Ying-dong, REN Ying-lei, QIU Ke-qiang. The catalytic performance of $\text{Cu}_{46}\text{Zr}_{47-x}\text{Al}_7\text{Y}_x$ amorphous ribbons in the degradation of AO II dye wastewater [J]. Environmental Science and Pollution Research, 2021, 28: 48038–48052.

$\text{Mg}_{65}\text{Cu}_{25-x}\text{Ag}_x\text{Y}_{10}$ 纳米多孔脱合金条带对 农药废水的降解率

夏青, 何诗瑶, 张伟, 向青春, 曲迎东, 任英磊, 邱克强

沈阳工业大学 材料科学与工程学院, 沈阳 110870

摘要: 为了提高农药废水的降解率, 利用淬态条带 $\text{Mg}_{65}\text{Cu}_{25-x}\text{Ag}_x\text{Y}_{10}$ ($x=0, 5, 10$, 摩尔分数, %) 稀硫酸脱合金化方法在其表面形成一层纳米孔径网状结构。与淬态条带相比, 这种结构的脱合金条带由于具有较大的比表面积和多的活性位点数, 表现出对农药废水具有更高的降解效率。其纳米多孔结构的平均孔径和降解率随着合金成分中 Ag 含量的增加而增大。在 pH=3、初始顺式氯菊酯浓度为 500 mg/L、条带用量为 1.33 g/L 的最佳条件下, $\text{Mg}_{65}\text{Cu}_{15}\text{Ag}_{10}\text{Y}_{10}$ 脱合金条带对农药废水最高降解率达到 95.8%。

关键词: 网状纳米多孔结构; MgCu 基非晶条带; 脱合金化; 顺式氯氰菊酯废水; 降解效率

(Edited by Bing YANG)